International Journal of Bioprinting

RESEARCH ARTICLE

The biological properties of 3D-printed degradable magnesium alloy WE43 porous scaffolds via the oxidative heat strategy

Shuyuan Min[1,2†], Chaoxin Wang[1,2†], Bingchuan Liu[1,2], Jinge Liu[3], Yu Liu[1,2], Zehao Jing[1,2], Yan Cheng[4], Peng Wen[3*], Xing Wang[5*], Yufeng Zheng[6], Yun Tian[1,2*]

[1]Department of Orthopedics, Peking University Third Hospital, Beijing 100191, People's Republic of China

[2]Engineering Research Center of Bone and Joint Precision Medicine, Ministry of Education, Beijing 100191, People's Republic of China

[3]Department of Mechanical Engineering, Tsinghua University, Beijing, 100084, China

[4]Biomed-X Center, Academy for Advanced Interdisciplinary Studies, Peking University, Beijing, 100871, China

[5]Beijing National Laboratory for Molecular Sciences, Institute of Chemistry, Chinese Academy of Sciences, Beijing 100190, China

[6]School of Materials Science and Engineering, Peking University, Beijing, 100871, China

(This article belongs to the *Special Issue: Additive Manufacturing of Functional Biomaterials*)

Abstract

As a biodegradable material, magnesium alloy has a modulus similar to that of bone, and given the biological activity of its degradation products, it has the potential to be a bone grafting material. Oxidation heat treatment is a very effective passivation method that may reduce the rate of magnesium alloy degradation. Oxidation heat treatment increases the rare earth oxide content of the scaffold as well as the corrosion resistance of the scaffold. The overall cytotoxicity of the as-printed scaffolds (APSs) and oxidation heat-treated scaffolds (OHSs) showed that OHSs accelerated cell proliferation. In the apoptosis experiment, the OHS group had a cell survival rate between that of the control group and of the as-printed group. In the osteogenic induction experiment, the alkaline phosphatase activity and the quantity of mineralized nodules were greater in the APS and OHS groups than in the control group. Marker proteins for bone growth were expressed at higher levels in the APS and OHS groups than in the control group. Therefore, oxidation heat-treated 3D printing scaffolds with good biocompatibility and osteogenic properties have great potential to be made into advanced biomaterials that can be used to fix bone defects.

Keywords: Oxidation heat; 3D printing; WE43 alloy; Magnesium alloy; Bone graft

†These authors contributed equally to this work.

***Corresponding authors:**
Yun Tian (tiany@bjmu.edu.cn)
Peng Wen (wenpeng@tsinghua.edu.cn)
Xing Wang (wangxing@iccas.ac.cn)

Citation: Min S, Wang C, Liu B, *et al*., 2023, The biological properties of 3D-printed degradable magnesium alloy WE43 porous scaffolds via the oxidative heat strategy. *Int J Bioprint,* 9(3): 686. https://doi.org/10.18063/ijb.686

Received: August 11, 2022
Accepted: November 08, 2022
Published Online: February 15, 2023

1. Introduction

Over 2 million bone grafting surgeries are performed each year worldwide[1]. While autologous bone is universally recognized as the best bone graft option available, but this technique can cause secondary trauma to the patient, and the allografts may cause immunological rejection and increase the risk of infectious diseases[2]. Therefore, it is

very important to find a more suitable bone substitute. Some artificial bone materials, such as calcium phosphate and calcium sulfate bone cements, can fill bone defects but lack biological activities, e.g., osteoinduction and durable mechanical support[3]. External fixator distraction osteogenesis can repair defects of the diaphysis of the extremities, but the repair may take a long time and it is difficult to repair the metaphysis due to anatomical mismatch[4]. In recent years, 3D printing technology has been used to prepare medical implants and biological organs[5], which can make prostheses personalized to the patient, achieve good anatomical shape matching, and control the elastic modulus by adjusting the printing parameters (structures, porosity, etc.) to repair large-segment bone defects and achieve the desired clinical effect[6,7]. However, currently, 3D printing still uses Ti6Al4V as the main component. Due to its nonabsorbability, the relative stability between bone and prosthesis and the long-term effects of stress conduction are uncertain and remain to be observed[8,9]. A bone defect filling material with overall strong support, osteoinductive ability, and biodegradability over time is urgently needed in the treatment of bone defects in limbs with 3D-printed prostheses.

Among biodegradable bioactive metals, magnesium and magnesium alloys have broad application prospects in orthopedic repair and reconstruction. The compression screw MAGNEZIX® developed by Syntellix AG, with the magnesium alloy WE43 as the main component, has been successfully applied in clinical practice, e.g., fracture fixation, and it presents biodegradable and osteogenic properties[10]. Magnesium is an element that is required for the proper functioning of the human body and is involved in a large variety of different biological processes. The beneficial role of magnesium ions in the development of bone has been proven in a number of *in vivo* and *in vitro* studies, and it has been found that magnesium alloys can increase the expression of alkaline phosphatase (ALP) in osteoblasts[11-13]. For example, Li *et al.* showed that the number of osteoblasts around magnesium alloy implants was significantly increased compared to the number around titanium implants[14]. He *et al.* used different concentration gradients (0–3 mM) of magnesium ions to culture human osteoblasts *in vitro* and found that the proliferative and osteogenic effects of magnesium ions on osteoblasts increased with increasing concentration[15].

However, the rapid degradation rate of WE43 magnesium alloy is a hindrance to its clinical application. Whether the oxide generated by metal oxidation can reduce the pace of WE43 magnesium alloy deterioration depends on the Pilling–Bedworth's ratio (PBR). PBR is used to quantify the passivation impact of metal oxides, which is defined as the volumetric ratio of the surface oxide to the metal consumed to create the metal oxide. A PBR less than 1 indicates that the metal oxide has weak passivation, while a PBR larger than 2 indicates that the oxide is easily peeled off and that the passivation is poor. When the PBR is greater than 1 and less than 2, the metal oxide has a significant passivation effect and may create a protective layer to prevent corrosion of the matrix metal. The oxidation of magnesium can generate MgO with a PBR of 0.81, which cannot slow its degradation rate[16], while the PBR values of Nd_2O_3, Y_2O_3 and Gd_2O_3 are 1.0584, 1.1923, and 1.29, respectively[17,18]. Moreover, Y, Nd, and Gd are more reactive than Mg, so they preferentially react with oxygen at high temperatures, forming a thin oxide layer on the surface. At present, microarc oxidation and phosphate coating of magnesium alloys have been widely studied, which can indeed significantly slow down the degradation rate of magnesium alloys[19,20]. However, the complicated process requires the use of specific instruments. For porous structures, it is not easy to use microarc oxidation to uniformly modify the surface of prostheses. In our previous studies[21], oxidation heat treatment is a very cost-effective and simple passivation method. Under a high-temperature oxidizing atmosphere, the degradable magnesium alloy undergoes a controllable oxidation reaction, and on the surface, a thick layer of passivation will eventually develop, which effectively isolates magnesium alloy and body fluid and slows the degradation rate of magnesium alloy medical implants in a body fluid environment[22]. However, no literature has investigated the effects of thermal oxidation treatment on the biocompatibility, and osteogenic properties of magnesium alloys. Therefore, in this work, thermal oxidation-treated WE43 magnesium alloy and as-printed WE43 were used to explore the differences in biocompatibility and osteogenic properties.

2. Materials and methods

2.1. Scaffold manufacturing and oxidation heat treatment

The scaffold was facilitated with laser powder bed fusion (L-PBF) using a compact L-PBF machine (BLT S210, China). The WE43 powder was prepared using centrifugal atomization (Tangshan Weihao, China). The powder was composed of 3.87% Y, 2.24% Nd, 1.16% Gd, 0.39% Zr, and residual Mg (in mass). The scaffolds were created with a pore size of 800 μm and a porosity of 60.0% as per design. The scaffold manufacturing protocol has been reported previously[23]. The scaffolds used in our experiments were cylindrical with the sheet gyroid structure and the strut size is 600 μm. The size was Φ10 mm × 10 mm. A 1-h preheating at 200°C was performed on the WE43 powder bed before the melting process. The processing chamber for the L-PBF process was filled with argon that had a purity

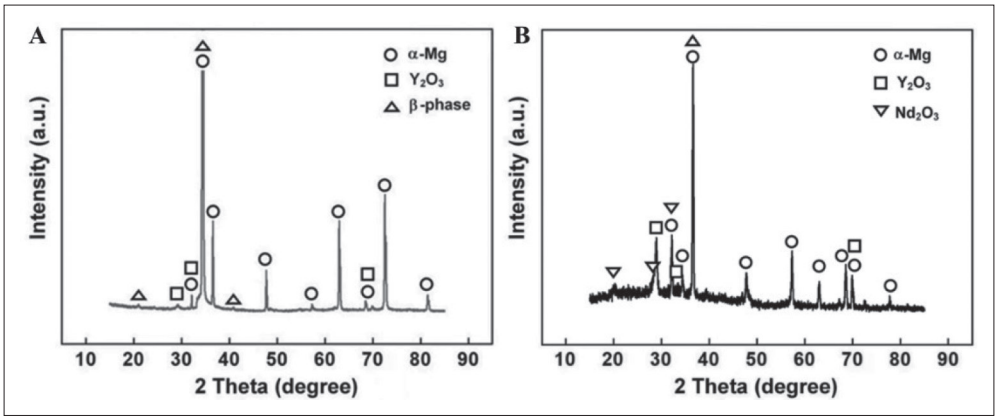

Figure 1. XRD results of (A) WE43 magnesium alloy APSs and (B) WE43 magnesium alloy OHSs. Scanning range: 10–90°; scanning speed 4°/min.

above 99.99%. The chamber was argon-filled during the L-PBF procedure, and to maintain a safe environment, the oxygen level was kept at or below 100 ppm. The specifics of the processing were as follows: 60 W laser power, 600 mm/s scanning speed, 20 μm layer thickness, and 70 μm hatch spacing. The scanning direction was flipped by 67° between adjacent layers. The postprocessing treatment of the as-printed scaffold (APS) was as follows. The scaffolds were chemically polished for 2 min by a solution of 5% HCl, 5% HNO_3, and balance C_2H_5OH (by volume) and then ultrasonically cleaned in pure ethyl alcohol. The samples were oxidation heat-treated at 525°C in a muffle furnace for 8 h and then water-quenched. The general structure of APS group and OHS group is shown in Figure S1.

2.2. X-ray diffraction

X-ray diffraction (XRD) (PANalytical, Netherlands) was used to accomplish phase identification in continuous scan mode at 40 kV and 200 mA. A rapid scan in the range of 10–90° was carried out at a rate of 4°/min so that a broad comprehension of the diffraction peaks could be obtained.

2.3. Preparation of extracts

The medium used for cell culture and extraction preparation was MEM-α (Lonza, Switzerland) containing 10% fetal bovine serum (Gibco, USA) and 1% penicillin-streptomycin (Gibco, USA). The extract was prepared according to ISO 10993-5:2009. The extraction preparation was performed at 37°C for 24 h. The mass/volume ratio was 0.1 g of test material per milliliter. The pH of the sample extract was adjusted to 7.4. One milliliter of complete leaching solution was placed into the super microwave digestion system (Milestone, Italy), and then 1 mL of nitric acid was added for digestion and diluted to 20 mL after completion. The ionic concentrations of the magnesium alloy components of the solutions, namely Mg, Gd, N, and Y, were tested by inductively coupled plasma atomic emission spectroscopy (ICP–AES) (Leeman, USA). The average was taken after three tests.

2.4. Cytotoxicity

Sprague Dawley rat bone marrow mesenchymal stem cells (BMSCs) (Procell, China) were seeded on 48-well plates (Corning, USA) with 1×10^4 cells per well, three parallel wells for each group, and 500 μL of medium per well. Then, the cells were allowed to grow in the culture environment for 24 h to allow them to adhere. After that, the control group was cultured with complete medium, and the experimental group was cultured with 100% and 50% APS and OHS extract. The medium was changed every 3 days.

CCK-8 experiments were carried out on days 1, 3, and 7. Before testing, the medium was exchanged in each well. To change the medium, the medium was aspirated. After the cells were washed with phosphate-buffered saline (PBS) three times, 500 μL of complete medium was added to the medium to make the necessary adjustments. Under dark conditions, each well received an additional 50 μL of the CCK-8 reagent (Dojindo, Japan), and three parallel blank controls were prepared at the same time. After putting the plate into an incubator (Thermo Fisher Scientific, USA) at a constant temperature (37°C, 5% CO_2) and leaving it there for 2 h, the absorbance at 450 nm was measured using a microplate reader (BioTek, Germany).

The cells were washed twice with PBS on day 7, the PBS was collected and mixed with the medium, the necessary quantity of trypsin was added, and when the cells were ready, they were placed in an incubator set with a constant temperature at 37°C with 5% CO_2. After 5 min, the cells were observed to determine whether they were successfully digested. If not, the digestion time was appropriately extended. An appropriate amount of complete medium was added to terminate the digestion, and a sterile Pasteur pipette was used to tap the bottom of the culture plate. At 4°C, the cell suspension was collected and centrifuged for

5 min at 1000 rpm. The cells were centrifuged after being rinsed twice with precooled PBS, and the supernatant was discarded after separation. Following the removal of the supernatant, the cells were resuspended in 100 μL of binding buffer. The 10× binding buffer was a concentrate composed of 0.2 μm sterile-filtered 0.1 M HEPES (pH 7.4), 1.4 M NaCl, and 25 mM $CaCl_2$ solution. The 10× buffer was diluted to 1× with ultrapure water. Finally, 10 μL of propidium iodide (PI) staining solution and 5 μL of annexin V-FITC (Yeasen, China) were used to stain the samples, and the samples were left at room temperature for 10–15 min away from light. Then, 400 μL of 1× binding buffer was added, each solution was mixed well and stored on ice, and a flow cytometer (Beckman Coulter, USA) was used for measurement.

2.5. Cell morphology

Seeding densities of 1×10^4 cells/disk were used for the BMSCs for up to 24 h of culture on WE43 and heat-treated WE43. After incubation, the samples were washed in phosphate buffer, fixed in 2.5% glutaraldehyde, dehydrated in a series of ethanol concentrations (50, 70, 80, 90, 95, 99, and 100%), subjected to critical point drying, and then coated with gold by sputtering. Next, field emission scanning electron microscopy (FESEM) was used to examine the samples.

2.6. ALP activity

Three groups were used in the experiment: the control group, the APS group, and the OHS group. In 24-well plates, BMSCs were cultured at a density of 2×10^4 mL^{-1}. Dexamethasone, L-ascorbic acid, and β-glycerophosphate (Sigma-Aldrich, USA) were added to the total medium, APS and OHS extract to reach concentrations of 8–10 M dexamethasone, 5 mg/mL L-ascorbic acid, and 5 mM β-glycerophosphate soon after incubation for a day, and the medium was exchanged. After that, the frequency of changing the medium was the same as that of the cytotoxicity test. On the 14th day, cells were lysed with radioimmunoprecipitation assay buffer (Lablead, China), and the lysate was added to a 96-well plate, followed by p-nitrophenyl phosphate (pNpp). ALP can catalyze the reaction of pNpp to generate p-nitrophenol, with the strongest absorbance at a wavelength of 405 nm. To assess the ALP activity, a microplate reader was used to obtain the absorbance readings, and a standard curve was created using a standard. To determine the amount of total cellular protein, a BCA kit (Yeasen, China) was used.

2.7. Alizarin Red test

Three groups were used in the experiment: the control group, the APS group, and the OHS group. After being seeded in 25 cm^2 cell culture flasks, BMSCs were cultured for 24 h to allow them to adhere. Then, the culture conditions were the same as those in the ALP activity test. Tests were performed on day 21 of culture. The media was removed, and PBS was used to rinse the cells twice. Then, the samples were fixed for 30 min in a 4% paraformaldehyde solution. The fixative was disposed, and after going through two rounds of cleaning with PBS, the samples were stained with Alizarin Red.

2.8. Western blot analysis of osteogenic markers

By using Western blot analysis, we were able to evaluate the protein expression levels of COL-1, BMP2, RUNX2, and SP7. After separating identical amounts of protein (20 μg) using sodium dodecyl sulfate-polyacrylamide gel electrophoresis (SDS-PAGE) at a concentration of 10%, the separated proteins were then transferred to polyvinylidene fluoride (PVDF) membranes. Two hours of blocking in TBST with 50 g/L skim milk powder was followed by an overnight incubation at 4°C with primary antibodies. The primary antibodies included rabbit anti-rat COL1, anti-BMP2, anti-RUNX2, anti-SP7 monoclonal antibody (Abcam, UK), and anti-β-actin polyclonal antibody (Applygen, China). The membranes were subsequently stained with a secondary antibody against rabbit IgG (Invitrogen, USA) after three rounds of washing. The data were obtained using an ECL detection kit, and to measure the relative intensity of the protein bands, ImageJ software was used.

2.9. Statistical analysis

The SPSS 26.0 statistical package was used for the data analysis. The differences between pairs of groups were analyzed using *t*-tests for independent samples, while the differences involving three or more groups were analyzed using one-way analysis of variance (ANOVA) followed by Tukey's test.

3. Results

3.1. XRD

As shown in Figure 2, the main component of the as-printed WE43 is α magnesium; there are also some β phase, and the composition of Y_2O_3 is lower. In the composition of oxidation heat-treated WE43, in addition to the main component of α magnesium, there are more metal oxides, including Y_2O_3 and Nd_2O_3, and the peak value of Y_2O_3 is higher than that of the as-printed group. The β phase of oxidation heat-treated WE43 was also significantly reduced.

3.2. ICP-AES of the extracts

The Mg content in the APS extract was 17.13 ± 0.10 mM, and the Mg content in the OHS extract was 3.53 ± 0.02 mM. Gd, Nd, and Y in the diluents of the two diluents with a volume of 20 mL did not reach the detection limit of ICP-AES.

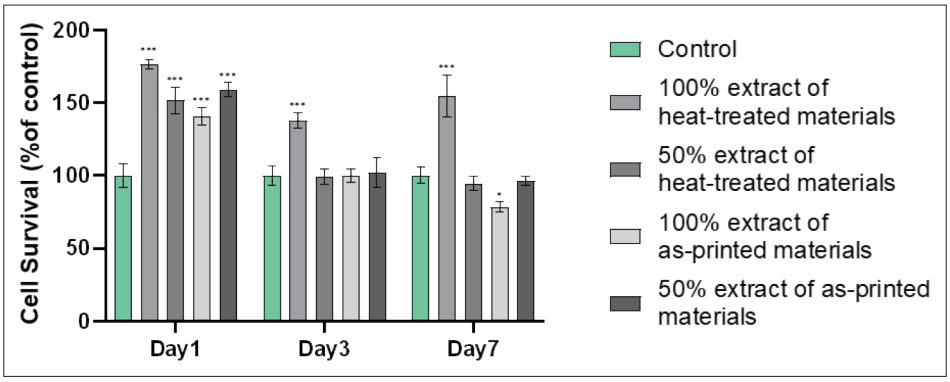

Figure 2. Cytotoxicity test by the CCK-8 method. Cell viability is shown as a function of time in culture (x-axis) and the number of days in culture, compared to the control group (y-axis). $^{*}P < 0.05$, $^{***}P < 0.001$ compared to the control group.

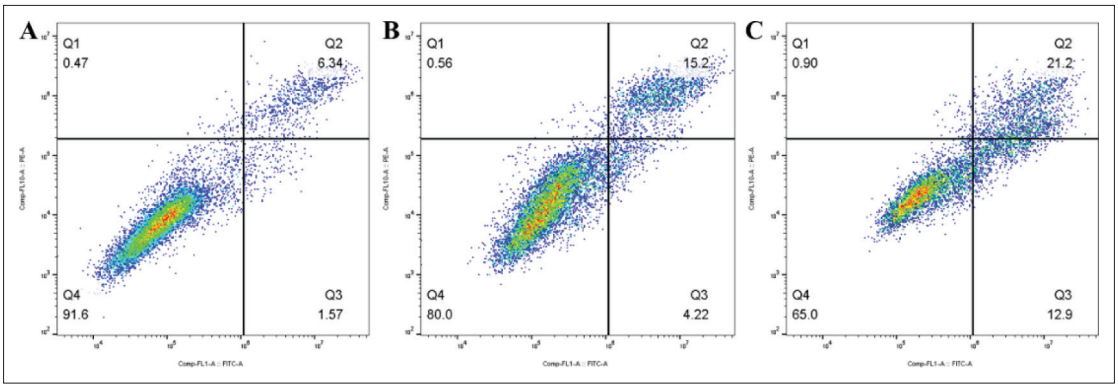

Figure 3. Apoptosis test. (A) The percentage of viable cells in the blank control group was 91.6%. (B) The percentage of viable cells in the OHS group was 80.0%. (C) The percentage of viable cells in the APS group was 65.0%.

3.3. Cytotoxicity test

As shown in Figure 2, when the extract was cultured for 1 day, there was a significant improvement in cell survival of the 100% and 50% extract OHS groups and the APS groups compared to the control group. Statistical analysis showed that after 3 days of extract culture, the cell survival rate was much greater in the 100% extract OHS group than in the control group. There was a statistically significant difference in the cell survival rates of the 100% extract OHS group and the control group after 7 days of extract culture. On day 7, cell viability in the 100% extract was lower in the APS group than in the control group.

3.4. Apoptosis test

As shown in Figure 3, flow cytometry revealed that compared to the experimental group, there were significantly more cells in the blank control group, which had not been stained with annexin V and PI. A total of 80.0% of cells were unstained in the OHS group, but only 65.0% were unstained in the APS group. The OHS group had fewer apoptotic and dead cells than the APS group. The number of cells in quadrants Q2 and Q3 in the APS group was greater than that in the other two groups, and the number of cells in quadrant Q1 did not show a significant difference. APS was more likely to induce apoptosis than OHS.

3.5. Cell morphology

As shown in Figure 4, BMSCs adhered and grew on the OHS, and compared to that of the APS, the number of adherent BMSCs on the OHS was much greater. Cell growth was not observed on most of the as-printed material.

3.6. ALP activity test

The ALP activity of each group was measured in diethanolamine (DEA) buffer after the protein quantitative treatment. Figure 5A demonstrates that the ALP activity of the control group was considerably different from both the APS group and OHS group, and the difference between the APS group and the OHS group was not statistically significant.

3.7. Alizarin Red test

After 21 days of induction culture, the cells of all three groups, as shown in Figure 5B, developed mineralized nodules, indicating that the three groups showed proper osteogenic differentiation. The APS group had a significantly greater density of mineralized nodules

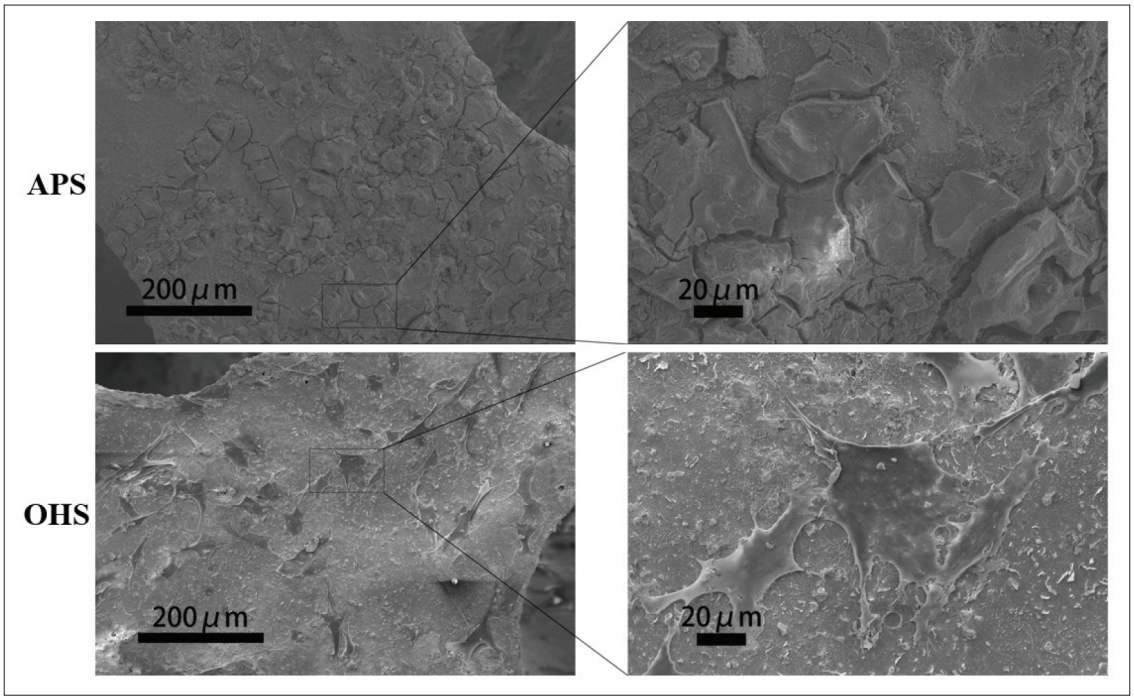

Figure 4. Morphology of BMSCs under FESEM. More BMSCs adhered and grew in the OHS group than in the APS group, which did not show cell growth.

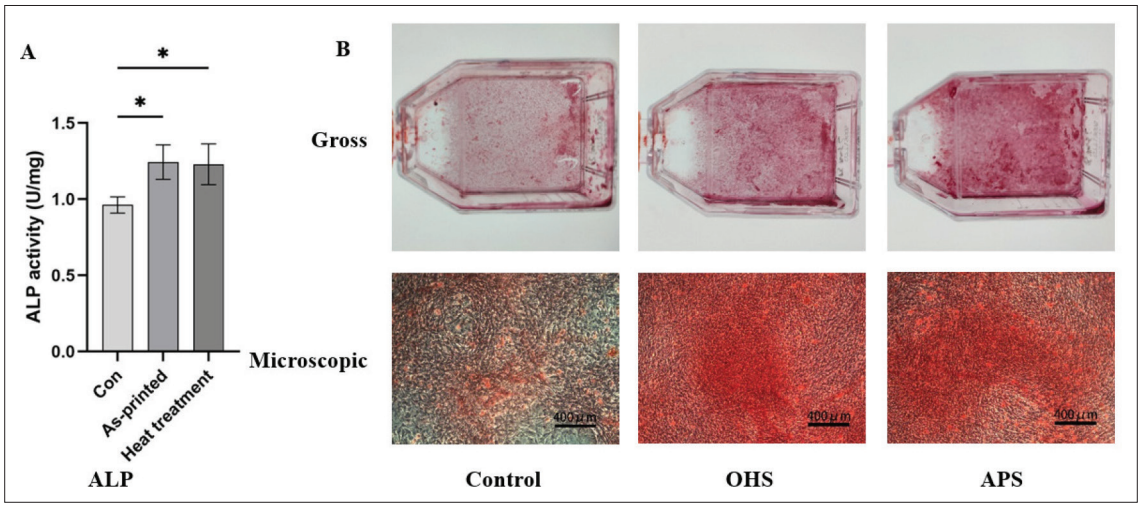

Figure 5. Osteogenic properties test. (A) The ALP activity of each group; (B) the gross and microscopic results of Alizarin Red staining. Mineralized nodules are stained red with Alizarin Red. *$P < 0.05$ for comparison between two groups.

than the OHS group. The mineralized nodules that were generated by extracellular calcium salt deposition were more common in the APS group and the OHS group than they were in the control group. However, extracellular calcium salt deposition was more noticeable in the APS group than in the OHS group.

3.8. Western blot analysis of osteogenic markers

As shown in Figure 6, among the cells of the three groups, the differences in the expression of each osteogenic marker protein were statistically significant. There was a statistically significant difference in the expression levels of the four proteins that were tested between the APS group and the control group. Except for RUNX2, there were significant differences in expression level of the other three proteins between the OHS group the control group. While there were no significant differences between the APS group and the OHS group in terms of COL1 and SP7, there were significant differences between the two groups in terms of RUNX2 and BMP2.

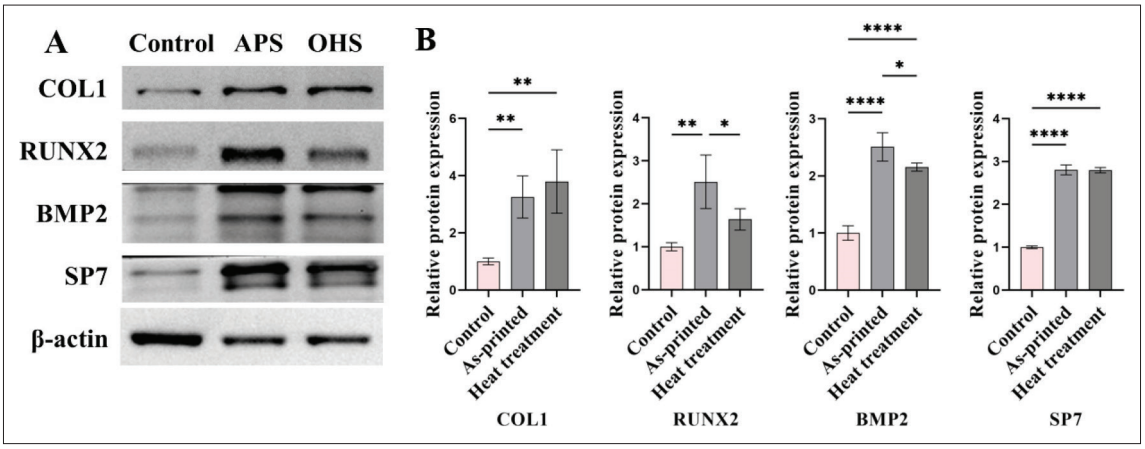

Figure 6. Western blotting of osteogenesis-related proteins. (A) Protein band map. (B) Protein semiquantitative results. *$P < 0.05$, **$P < 0.01$, ****$P < 0.0001$ for comparison between two groups.

4. Discussion

Magnesium alloy structures fabricated by additive manufacturing are expected to be effective supporting scaffolds in bone. The porous structure helps to reduce the mass of the alloy and the growth of the bone structure, but the increase in surface area also accelerates absorption. In recent years, research has focused on controlling the rate of magnesium alloy degradation. Since the PBR of magnesium is small, its degradation rate cannot be slowed down. Many prior studies have attempted to delay magnesium alloy degradation by coating, but this approach is not only expensive and difficult, but also prone to the introduction of harmful components. Other than being cost-effective, oxidation heat treatment does not change the elements of the alloy, which is beneficial to the safety of the alloy. This can cause the more highly reactive elements to form a layer of oxide that may be seen on the surface of the alloy, and on the prosthetic surface of the magnesium alloy, it is possible for the oxide film to develop in a homogeneous layer. Therefore, WE43 can form Y_2O_3 on the surface after oxidation heat treatment. As the results of our XRD experiments, the peaks of rare earth oxides increased after oxidative heat treatment, while the peaks of β phase decreased due to the formation of rare earth oxides on the surface. Compared to MgO, the rate of degradation of magnesium alloys can be effectively slowed down by the formation of Y_2O_3. It has been reported that increasing the composition of yttrium in magnesium alloys can form Y_2O_3, thereby reducing the degradation rate of magnesium alloys[24].

In terms of biocompatibility, no evident cytotoxicity was observed in APS or OHS. Only the 100% APS extract showed some cytotoxicity when cultured with cells for 7 days. For BMSCs, magnesium ions can promote cell proliferation within a certain range and improve osteogenesis, although they exhibit certain cytotoxicity at higher concentrations[25]. When cultured for a short time, each group was able to promote cell proliferation. APS had a faster degradation rate, and the magnesium in the extract exceeded the optimum concentration of magnesium needed to promote cell proliferation, showing a certain degree of toxicity after culturing for a week. The concentration of magnesium in the extract of OHS was much lower than that of the APS group, so at all three times, its rate of proliferation exceeded that of the control group. As a result of the lower magnesium ion concentration in the OHS group, the effect of the diluted extract on cell proliferation was not evident after 7 days of culture. In addition to magnesium, the rare earth element composition in the WE43 alloy may also influence its cytocompatibility. Previous literature has shown that ionized rare earth elements, including Y, Nd, and Gd, exhibit significant cytotoxicity at concentrations of approximately 1000 μM[26]. According to the literature, the detection limits of Y, Gd, and Nd are 0.2187 ppm, 0.4064 ppm, and 0.0405 ppm, respectively, indicating that the concentrations of Y, Gd, and Nd elements in the extract are less than 4.374 ppm, 8.128 ppm, and 0.81 ppm[27]. In this experiment, the rare earth element content in the extract was analyzed, and it was found that the concentration was below the detection limit of ICP-AES, far less than the concentration required for the rare earth elements to produce clear cytotoxicity. Thus, the *in vitro* results showed that rare earth elements had little effect on cytocompatibility.

In comparison to the blank control group and the OHS group, the number of cells in the Q2 and Q3 quadrants of the APS group was significantly higher, indicating that the cytotoxicity caused by the material mainly led to apoptosis, instead of necrosis. The number of surviving

BMSCs cultured in the OHS group was between that of the blank control group and of the APS group, which suggested that oxidation heat treatment could improve the biocompatibility.

ALP is an osteogenic molecule expressed by BMSCs and osteoblasts and is highly expressed in mineralized bone tissue[28]. It has been reported that the expression level of ALP in BMSCs cultured *in vitro* can be used to predict their osteogenic ability *in vivo*[29]. By measuring ALP activity, the ALP expression of both the APS and OHS groups was greater than that of the control group. In terms of the late phase of osteogenesis, this study used Alizarin Red staining, which can stain mineralized nodules red. Since mineralization is the result of late osteogenesis, Alizarin Red staining mainly reflects the level of late osteogenesis[30]. In Alizarin Red mineralized nodule staining, the OHS group also showed the best osteogenic properties. In the ALP test, the ability of the APS group to induce osteogenic differentiation was similar to that of the blank group, while in the Alizarin Red staining experiment, the APS group had a much greater density of mineralized nodules than the blank group. Combined with the results of the BCA kit, this may be due to the magnesium ions promoting cell proliferation and protein expression.

The RUNX2 protein is a transcription factor closely related to osteoblast differentiation. Expression of this gene is induced more strongly in preosteoblasts and immature osteoblasts than in mature osteoblasts[31]. It has been shown in the literature that magnesium salts can promote the expression of RUNX2 in murine BMSCs and promote their differentiation into osteoblasts. Using 0 mM and 20 mM magnesium ion medium, it was found that the cells cultured with 20 mM magnesium ion were more sensitive to RUNX2 than the cells cultured in 0 mM magnesium[32]. In this experiment, magnesium alloy bone implants were used, and it was intuitively observed that magnesium-rare earth alloys stimulated the expression of molecules involved in osteogenesis *in vitro*. Among them, the concentration of magnesium ion in the APS group was higher, approximately 17.13 mM, than that in the OHS group, which was approximately 3.53 mM, similar to the results of culturing cells with magnesium salts.

As a transcription factor, RUNX2 is also closely related to the regulation of the cell cycle. In mitosis, there is a correlation between RUNX2 and cyclin B1[33]. RUNX2 expression in the MC3T3-E1 osteoblast cell line was very high during the G1 phase of mitosis and relatively low during the S, G2, and M phases[34]. In addition, knockdown of RUNX2 also produces G1-related antiproliferative effects[35]. In conclusion, the expression of RUNX2 promotes cell proliferation. CCK-8 data showed that BMSC proliferation was greater in the OHS group than in the control group, which was related to the promotion of RUNX2 expression. From the microscopy images of Alizarin Red staining, in addition to having more mineralized nodules than the control group, the APS and OHS groups also had a greater cell density than the control group, which further shows that WE43 magnesium alloy could promote the proliferation of BMSCs to indirectly promote osteogenesis. In addition, the SP7 protein, or osterix, is a protein that acts as a transcription factor to stimulate the differentiation of BMSCs into osteoblasts and ultimately osteocytes[36]. This transcription factor is often utilized as a marker of osteoblast development since it acts in the transcriptional cascade after RUNX2. Mouse embryos with the SP7 gene knocked out have no bone formation[37]. BMP2 serves a crucial function in osteogenic differentiation induction. Previous literature has shown that RUNX2 is stabilized by BMP2-activated ERK/MAP kinase to promote osteoblast differentiation[38]. Increased SP7 and BMP2 expression compared to the control group was demonstrated by Western blotting in the APS and OHS groups, suggesting that WE43 magnesium alloy could promote osteogenesis through SP7 and BMP2. This study mainly focused on the effect of magnesium ion on the differentiation of BMSCs *in vitro*. In fact, magnesium ion promotes osteogenesis through additional mechanisms *in vivo*. For example, magnesium ions can promote the expression of calcitonin gene-related polypeptide-α in periosteal neurons, thereby promoting osteoblast differentiation[39]. Therefore, it is also expected that the scaffold has better osteogenesis *in vivo*.

5. Conclusion

In summary, we demonstrate an oxidation heat-treated WE43 magnesium alloy made by additive manufacturing, which possessed good biocompatibility, biodegradability, and superior osteogenic properties for clinical bone defect repair. The cytotoxicity of both APSs and OHSs was low and related to the induction of apoptosis. BMSCs are more likely to adhere and grow on OHSs. The osteogenic activities of the APSs and OHSs were better than those of the control group. During the culture process, the ALP activity of the APS and OHS groups was higher than that of the control. Compared to the control group, the scaffold groups expressed more of the upstream proteins RUNX2, SP7, and BMP2 and the downstream protein COL1. Thus, the scaffolds have the potential for future clinical applications in orthopedic implants, but further animal experiments and clinical studies are still needed to verify their efficacy in the future.

Acknowledgments

None.

Funding

This work was funded by the National Key Research and Development Program of China (2018YFE0104200), the Youth Innovation Promotion Association CAS (2019031), and the National Natural Science Foundation of China (51875310, 52175274, 82172065).

Conflict of interest

The authors declare no conflicts of interest.

Author contributions

Conceptualization: Yufeng Zheng, Peng Wen, Yun Tian
Data curation: Shuyuan Min, Chaoxin Wang
Formal analysis: Shuyuan Min, Chaoxin Wang
Methodology: Shuyuan Min
Investigation: Shuyuan Min, Chaoxin Wang, Bingchuan Liu, Jinge Liu, Yu Liu, Zehao Jing
Project administration: Yufeng Zheng, Peng Wen, Yun Tian
Supervision: Yun Tian
Validation: Yun Tian
Writing – original draft: Shuyuan Min, Chaoxin Wang
Writing – review & editing: Yan Cheng, Yufeng Zheng, Peng Wen, Xing Wang, Yun Tian

Ethics approval and consent to participate

Not applicable.

Consent for publication

Not applicable.

Availability of data

Not applicable.

References

1. Archunan MW, Petronis S, 2021, Bone grafts in trauma and orthopaedics. *Cureus*, 13(9):e17705.

   https://doi.org/10.7759/cureus.17705

2. Grambart ST, Anderson DS, Anderson TD, 2020, Bone grafting options. *Clin Podiatr Med Surg*, 37(3):593–600.

   https://doi.org/10.1016/j.cpm.2020.03.012

3. Šupová M, 2015, Substituted hydroxyapatites for biomedical applications: A review. *Ceram Int*, 41(8):9203–9231.

   https://doi.org/10.1016/j.ceramint.2015.03.316

4. Kani KK, Porrino JA, Chew FS, 2020, External fixators: Looking beyond the hardware maze. *Skelet Radiol*, 49(3):359–374.

   https://doi.org/10.1007/s00256-019-03306-w

5. Yi-Wu J, Hsieh CH, Lin ZY, 2022, Novel high-speed 3D printing method using selective oil sintering with thermoplastic polyurethane powder printing. *Int J Bioprint*, 8(2):521.

   https://doi.org/10.18063/ijb.v8i2.521

6. Yin C, Zhang T, Wei Q, *et al.*, 2022, Surface treatment of 3D printed porous Ti6Al4V implants by ultraviolet photofunctionalization for improved osseointegration. *Bioactive Mater*, 7:26–38.

   https://doi.org/10.1016/j.bioactmat.2021.05.043

7. Kadakia RJ, Wixted CM, Allen NB, *et al.*, 2020, Clinical applications of custom 3D printed implants in complex lower extremity reconstruction. *3D Print Med*, 6(1):29.

   https://doi.org/10.1186/s41205-020-00083-4

8. Deng F, Liu L, Li Z, *et al.*, 2021, 3D printed Ti6Al4V bone scaffolds with different pore structure effects on bone ingrowth. *J Biol Eng*, 15(1):4.

   https://doi.org/10.1186/s13036-021-00255-8

9. Sumner DR, 2015, Long-term implant fixation and stress-shielding in total hip replacement. *J Biomech*, 48(5):797-800.

   https://doi.org/10.1016/j.jbiomech.2014.12.021

10. Biber R, Pauser J, Gesslein M, *et al.*, 2016, Magnesium-based absorbable metal screws for intra-articular fracture fixation. *Case Rep Orthop*, 2016:9673174.

    https://doi.org/10.1155/2016/9673174

11. Leem YH, Lee KS, Kim JH, *et al.*, 2016, Magnesium ions facilitate integrin alpha 2- and alpha 3-mediated proliferation and enhance alkaline phosphatase expression and activity in hBMSCs. *J Tissue Eng Regen Med*, 10(10):E527–E536.

    https://doi.org/10.1002/term.1861

12. Chen K, Xie X, Tang H, *et al.*, 2020, In vitro and in vivo degradation behavior of Mg-2Sr-Ca and Mg-2Sr-Zn alloys. *Bioact Mater*, 5(2):275–285.

    https://doi.org/10.1016/j.bioactmat.2020.02.014

13. Xia D, Liu Y, Wang S, *et al.*, 2018, In vitro and in vivo investigation on biodegradable Mg-Li-Ca alloys for bone implant application. *Sci China Mater*, 62(2):256–272.

    https://doi.org/10.1007/s40843-018-9293-8

14. Li Z, Gu X, Lou S, *et al.*, 2008, The development of binary Mg–Ca alloys for use as biodegradable materials within bone. *Biomaterials*, 29(10):1329–1344.

    https://doi.org/10.1016/j.biomaterials.2007.12.021

15. He LY, Zhang XM, Liu B, *et al.*, 2016, Effect of magnesium ion on human osteoblast activity. *Braz J Med Biol Res*, 49(7): e5257.

https://doi.org/10.1590/1414-431X20165257

16. Yang Y, He C, Dianyu E, *et al.*, 2020, Mg bone implant: Features, developments and perspectives. *Mater Design*, 185:108259.

https://doi.org/10.1016/j.matdes.2019.108259

17. Jiang Q, Lu D, Liu C, *et al.*, 2021, The Pilling-Bedworth ratio of oxides formed from the precipitated phases in magnesium alloys. *Front Mater*, 8:761052.

https://doi.org/10.3389/fmats.2021.761052

18. Kim YM, Yim CD, Kim HS, *et al.*, 2011, Key factor influencing the ignition resistance of magnesium alloys at elevated temperatures. *Script Mater*, 65(11):958–961.

https://doi.org/10.1016/j.scriptamat.2011.08.019

19. Wu Y, Wang YM, Zhao DW, *et al.*, 2019, In vivo study of microarc oxidation coated Mg alloy as a substitute for bone defect repairing: Degradation behavior, mechanical properties, and bone response. *Colloids Surf B Biointerfaces*, 181:349–359.

https://doi.org/10.1016/j.colsurfb.2019.05.052

20. Lalk M, Reifenrath J, Angrisani N, *et al.*, 2013, Fluoride and calcium-phosphate coated sponges of the magnesium alloy AX30 as bone grafts: A comparative study in rabbits. *J Mater Sci Mater Med*, 24(2):417–436.

https://doi.org/10.1007/s10856-012-4812-2

21. Liu J, Yin B, Song F, *et al.*, 2022, Improving corrosion resistance of additively manufactured WE43 magnesium alloy by high temperature oxidation for biodegradable applications. *J Magnes Alloys*.

https://doi.org/10.1016/j.jma.2022.08.009

22. Bar F, Berger L, Jauer L, *et al.*, 2019, Laser additive manufacturing of biodegradable magnesium alloy WE43: A detailed microstructure analysis. *Acta Biomater*, 98:36–49.

https://doi.org/10.1016/j.actbio.2019.05.056

23. Liu J, Liu B, Min S, *et al.*, 2022, Biodegradable magnesium alloy WE43 porous scaffolds fabricated by laser powder bed fusion for orthopedic applications: Process optimization, in vitro and in vivo investigation. *Bioact Mater*, 16:301–319.

https://doi.org/10.1016/j.bioactmat.2022.02.020

24. Zhang Q, Li Q, Chen X, 2020, Effect of heat treatment on corrosion behavior of Mg–5Gd–3Y–0.5Zr alloy. *RSC Adv*, 10(71):43371–43382.

https://doi.org/10.1039/d0ra08933h

25. Lu WC, Pringa E, Chou L, 2017, Effect of magnesium on the osteogenesis of normal human osteoblasts. *Magnes Res*, 30(2):42–52.

https://doi.org/10.1684/mrh.2017.0422

26. Feyerabend F, Fischer J, Holtz J, *et al.*, 2010, Evaluation of short-term effects of rare earth and other elements used in magnesium alloys on primary cells and cell lines. *Acta Biomater*, 6(5):1834–1842.

https://doi.org/10.1016/j.actbio.2009.09.024

27. Li F, Gong A, Qiu L, *et al.*, 2017, Simultaneous determination of trace rare-earth elements in simulated water samples using ICP-OES with TODGA extraction/back-extraction. *PLoS One*, 12(9):e0185302.

https://doi.org/10.1371/journal.pone.0185302

28. Vimalraj S, 2020, Alkaline phosphatase: Structure, expression and its function in bone mineralization. *Gene*, 754:144855.

https://doi.org/10.1016/j.gene.2020.144855

29. Prins HJ, Braat AK, Gawlitta D, *et al.*, 2014, In vitro induction of alkaline phosphatase levels predicts in vivo bone forming capacity of human bone marrow stromal cells. *Stem Cell Res*, 12(2):428–440.

https://doi.org/10.1016/j.scr.2013.12.001

30. Dubey N, Bentini R, Islam I, *et al.*, 2015, Graphene: A versatile carbon-based material for bone tissue engineering. *Stem Cells Int*, 2015:804213.

https://doi.org/10.1155/2015/804213

31. Komori T, 2009, Regulation of osteoblast differentiation by Runx2. Osteoimmunology. *Adv Exp Med Biol*, 658:43–49.

32. Arumugam B, Vishal M, Shreya S, *et al.*, 2019, Parathyroid hormone-stimulation of Runx2 during osteoblast differentiation via the regulation of lnc-SUPT3H-1:16 (RUNX2-AS1:32) and miR-6797-5p. *Biochimie*, 158:43-52.

https://doi.org/10.1016/j.biochi.2018.12.006

33. Qiao M, Shapiro P, Fosbrink M, *et al.*, 2006, Cell cycle-dependent phosphorylation of the RUNX2 transcription factor by cdc2 regulates endothelial cell proliferation. *J Biol Chem*, 281(11):7118–7128.

https://doi.org/10.1074/jbc.M508162200

34. San Martin IA, Varela N, Gaete M, *et al.*, 2009, Impaired cell cycle regulation of the osteoblast-related heterodimeric transcription factor Runx2-Cbfbeta in osteosarcoma cells. *J Cell Physiol*, 221(3):560–571.

https://doi.org/10.1002/jcp.21894

35. Galindo M, Pratap J, Young DW, *et al.*, 2005, The bone-specific expression of Runx2 oscillates during the cell cycle to support a G1-related antiproliferative function in osteoblasts. *J Biol Chem*, 280(21):20274–20285.

https://doi.org/10.1074/jbc.M413665200

36. Sinha KM, Zhou X, 2013, Genetic and molecular control of osterix in skeletal formation. *J Cell Biochem*, 114(5):975–984.

https://doi.org/10.1002/jcb.24439

37. Nakashima K, Zhou X, Kunkel G, *et al.*, 2002, The novel zinc finger-containing transcription factor osterix is required for osteoblast differentiation and bone formation. *Cell*, 108(1):17–29.

https://doi.org/10.1016/s0092-8674(01)00622-5

38. Jun JH, Yoon WJ, Seo SB, *et al.*, 2010, BMP2-activated Erk/MAP kinase stabilizes Runx2 by increasing p300 levels and histone acetyltransferase activity. *J Biol Chem*, 285(47):36410–36419.

https://doi.org/10.1074/jbc.M110.142307

39. Yang Y, Rao J, Liu H, *et al.*, 2022, Biomimicking design of artificial periosteum for promoting bone healing. *J Orthop Transl*, 36:18–32.

https://doi.org/10.1016/j.jot.2022.05.013